

## **Amplitude responses of thin beds : sinusoidal approximation versus Ricker approximation**

Hai-Man Chung and Don C. Lawton

### **ABSTRACT**

The amplitude responses of thin beds whose thicknesses are below  $(1/8)\lambda_d$ , where  $\lambda_d$  is the predominant wavelength, are studied. Two analytical expressions for the amplitude response as a function of the thickness are derived. The first one is based on the substitution of a sine wave for the input wavelet, and the second one is based directly on the analytical expression for the Ricker zero-phase wavelet. The numerical results of these two expressions are compared to the numerical results of several models. It is found that below  $(1/8)\lambda_d$ , the differences between the two expressions are very small, and both are good approximations, assuming that the limit of good agreement between the analytical results and the modelling results is about 10%. Above the  $(1/8)\lambda_d$  thickness, the percentage differences increase rapidly for both expressions, implying that the thin-bed assumptions in both derivations breaks down rapidly beyond the  $(1/8)\lambda_d$  thickness.

### **INTRODUCTION**

One approach to defining a thin bed is the linearity limit of the functional behavior of the amplitude of the reflected composite wavelet as a function of the thickness of the bed. By approximating a wavelet peak with the peak of a monochromatic sine wave whose wavelength is equal to the predominant wavelength of the wavelet, Widess (1973) derived the following expression:

$$A_d = \frac{4\pi A_i r b}{\lambda_d} \quad (a)$$

where  $A_d$  = the amplitude of the composite wavelet

$A_i$  = the mean amplitude of the maximum peak and trough of the input wavelet

$r$  = the magnitude of the reflection coefficients

$b$  = the thin-bed thickness

$\lambda_d$  = the predominant wavelength in the thin bed

The above expression simply says that, for thin beds, the amplitude of the reflection is approximately proportional to the thickness of the bed and inversely proportional to the

predominant wavelength. Indirectly, Widess defined a thin bed as a bed whose thickness is such that the amplitude of a composite reflection obeys the above expression. Koefoed and de Voogd (1980) considered thin layers from the point of view of the quasi-linear relation that exists between their thickness and their reflection amplitude to a seismic signal. They considered that a bed is thin if the amplitude response as a function of thickness deviates less than 10% from a linear relationship. Using an integral representation of a wavelet, de Voogd and den Rooijen (1983) derived the following results for a thin bed:

$$b(x, t) = \frac{r\zeta}{1-r^2} a'(x, t) \tag{b}$$

- where  $b(x, t)$  = the composite wavelet
- $a'(x, t)$  = the first derivative of the input wavelet  $a(x, t)$  with respect to time
- $r$  = the reflection coefficient
- $z$  = the 2-way travel time in layer

They concluded that a thin layer is a layer whose composite reflection has the shape of the first derivative of the wavelet and that its amplitude is proportional to the thickness of the layer and to a factor depending upon the reflection coefficient of a single interface. Note that Widess, Koefoed, de Voogd, and den Rooijen only considered vertical plane waves incident upon two equal-amplitude spikes with opposite polarities. Hence, their conclusions cannot be considered general.

In the following sections, two analytical expressions for the amplitude behavior of a thin bed as a function of thickness are derived. The first expression is an extension of Widess' method, and is based on a sinusoidal approximation. The second expression is derived directly from the expression of a Ricker zero-phase wavelet. The only approximation in this expression is the thin-bed assumption. The results from these two expressions will be discussed and compared. Note that in deriving both equations transmission loss and internal multiples are ignored. As pointed out by Koefoed and de Voogd (1980), such effects are negligible as long as the acoustic impedance ratio between the thin layer and the surrounding rock lies between the bounds of 0.5 and 2, which they also pointed out is the range of acoustic contrast usually encountered in practice. In our examples, the acoustic impedance ratio ranges from 0.75 (model 1B) to 1.52 (model 1A).

### **SINUSOIDAL APPROXIMATION**

Consider a thin bed embedded in an infinitely homogeneous medium. Let  $r_1$  and  $r_2$  be the reflection coefficients of the upper and lower interfaces respectively. Following Widess' (1973) approach, to the first order of approximation, the central portion of a Ricker zero-phase wavelet can be approximated by a sine wave whose wavelength is equal

to the predominant wavelength of the wavelet. Choosing the centre of the thin bed as the zero time reference and assuming a Ricker zero-phase wavelet as the input wavelet, the maximum amplitude of the reflected composite wavelet can be approximated as:

$$A_r = A_i r_1 \cos \left[ \left( t + \frac{b}{V} \right) \frac{2\pi}{T_d} \right] + A_i r_2 \cos \left[ \left( t - \frac{b}{V} \right) \frac{2\pi}{T_d} \right] \quad (1)$$

where  $A_i$  = the maximum amplitude of the sine wave  
 $b$  = the thickness of the thin bed  
 $V$  = the P-wave velocity within the thin bed  
 $T_d$  = the predominant period of the input Ricker zero-phase wavelet

Expanding the cosine terms, we have:

$$A_r = A_i (r_1 + r_2) \cos \frac{2\pi t}{T_d} \cos \frac{2\pi b}{\lambda_d} + A_i (r_2 - r_1) \sin \frac{2\pi t}{T_d} \sin \frac{2\pi b}{\lambda_d}$$

where  $\lambda_d$  = the predominant wavelength of the input wavelet

Now, we make the thin bed approximation. For sufficiently small  $b$ ,  $\sin \frac{2\pi b}{\lambda_d} = \frac{2\pi b}{\lambda_d}$  and

$$\cos \frac{2\pi b}{\lambda_d} = 1 - 2 \left( \sin \frac{\pi b}{\lambda_d} \right)^2 \approx 1 - 2 \left( \frac{\pi b}{\lambda_d} \right)^2. \text{ Using these approximations, we can write:}$$

$$\begin{aligned} A_r &= A_i (r_1 + r_2) \left[ 1 - 2 \left( \frac{\pi b}{\lambda_d} \right)^2 \right] \cos \frac{2\pi t}{T_d} + A_i (r_2 - r_1) \frac{2\pi b}{\lambda_d} \sin \frac{2\pi t}{T_d} \\ &= M_1 \cos \frac{2\pi t}{T_d} + M_2 \sin \frac{2\pi t}{T_d} \end{aligned} \quad (2)$$

$$\text{where } M_1 = A_i (r_1 + r_2) \left[ 1 - 2 \left( \frac{\pi b}{\lambda_d} \right)^2 \right]$$

$$\text{and } M_2 = A_i (r_2 - r_1) \frac{2\pi b}{\lambda_d}$$

For maximum or minimum  $A_r$ ,  $\frac{dA_r}{dt} = 0$

$$\therefore \frac{dA_r}{dt} = 0 = -\frac{2\pi A_i}{T_d} M_1 \sin \frac{2\pi t}{T_d} + \frac{2\pi A_i}{T_d} M_2 \cos \frac{2\pi t}{T_d}$$

$$\Rightarrow \tan \frac{2\pi t}{T_d} = \frac{M_2}{M_1}$$

$$\Rightarrow t = \frac{T_d}{2\pi} \tan^{-1} \left( \frac{M_2}{M_1} \right)$$

Note that since we are using continuous sine waves to derive the above expression, there is actually more than one value of  $t$  that would give maximum or minimum value of

$A_r$ . A value of  $t$  given by the above expression plus  $\frac{n\pi}{\omega}$ , i.e.  $t + \frac{n\pi}{\omega}$ , where  $n$  is an integer and  $\omega$  is the angular frequency of the sine wave, will lead to either maximum or minimum value of  $A_r$ . But since we are interested only in the maximum and minimum value of  $A_r$  where  $t$  is closest to zero, we will only consider the case where  $n = 0$ .

Substituting this expression for  $t$  into equation (2), we obtain:

$$\begin{aligned} A_r &= M_1 \cos \frac{2\pi}{T_d} \left[ \frac{T_d}{2\pi} \tan^{-1} \left( \frac{M_2}{M_1} \right) \right] + M_2 \sin \frac{2\pi}{T_d} \left[ \frac{T_d}{2\pi} \tan^{-1} \left( \frac{M_2}{M_1} \right) \right] \\ &= M_1 \frac{M_1}{\sqrt{M_1^2 + M_2^2}} + M_2 \frac{M_2}{\sqrt{M_1^2 + M_2^2}} = \sqrt{M_1^2 + M_2^2} \end{aligned}$$

$$\therefore A_r = A_i \left\{ (r_1 + r_2)^2 \left[ 1 - 2 \left( \frac{\pi b}{\lambda_d} \right)^2 \right]^2 + (r_2 - r_1)^2 \left( \frac{2\pi b}{\lambda_d} \right)^2 \right\}^{\frac{1}{2}} \quad (3)$$

Equation (3) is the amplitude equation sought. Note that  $A_r$  has two roots, a positive root for the reflected composite wavelet peak, and a negative root for the trough. Since equation (3) is actually derived from the interference of two continuous sine waves with the same wavelength, the two roots obviously should be identical in magnitude due to symmetry. Therefore, we need only consider one of the roots. We will consider the positive root and refer to  $A_r$  as the absolute maximum amplitude.

Therefore, equation (3) gives the absolute maximum amplitude response of a thin bed for the general case. As shown by Widess (1973) and also in the next section, for equation (3) to be valid, the maximum thickness  $b$  is approximately  $1/8$  of the predominant wavelength. For  $r_1 = -r_2$ , the first term in the expression for  $A_r$  is zero and the second term becomes  $4\pi r_1 b A_i / \lambda_d$ , which is the expression derived by Widess (1973). For  $r_1 = r_2$ , the second term is zero and the first term becomes  $2A_i r_1 (1 - 2\pi^2 b^2 / \lambda_d^2)$ , which approaches a value of  $2A_i r_1$ , as  $b$  approaches zero, as expected. For  $|r_1| \neq |r_2|$ ,  $A_r$  receives contribution from both terms. Equation (3) also indicates that, except for the case of  $r_2 = -r_1$ , the absolute maximum amplitude of a composite wavelet reflected from a thin bed is not linearly proportional to the bed thickness, but rather, the relationship is a complicated second-ordered polynomial. This implies that in exploration seismic data, calibration of amplitude for a thin bed reflection to infer the thickness based on a linear relationship will lead to erroneous results unless  $r_2 = -r_1$ .

The fact that equation (3) is derived from using the approximation of a continuous sine wave leads to an interesting property. For a thin bed represented by two spikes of equal polarity, numerical results from equation (3) are close to modelling results one would obtain regardless whether the input wavelet is zero-phase or  $90^\circ$ -phase. However, if the spikes are of opposite polarity, equation (3) actually gives values that would result only from an input  $90^\circ$ -phase wavelet. The reason for this can be explained graphically as follows.

Consider the case of equal polarity. Figure 1a shows two identical sine waves separated by a distance less than  $1/8$  of its wavelength. Note that a convolution of a sine wave with two spikes can be obtained by simply summing two sine waves with the proper polarities and separated by the same distance between the spikes. Figure 1b shows the results of the summing of the two sine curves. The boxed portions of the curves in both Figures 1a and 1b indicate the corresponding areas before and after summing. If we compare these two boxes to the corresponding boxes areas in Figures 1c and 1d where a zero-phase input wavelet, whose predominant wavelength is equal to the wavelength of the sine wave, is used, one could see that they are very similar. Hence, equation (3) is a good approximation for the equal-polarity case with a zero-phase wavelet input. This will also be true if the input wavelet is  $90^\circ$ -phase, since the peak region of a Ricker  $90^\circ$ -phase wavelet has the same shape as that of a zero-phase wavelet.

Figures 2a, 2b, 2c and 2d show similar diagrams for the case of opposite polarity. It is quite clear from Figure 2a that the portions of the sine curves inside the box are quite different from that of the zero-phase wavelet in the box in Figure 2c. The much lower amplitude of the side lobe of the zero-phase wavelet results in this difference. However, in Figure 2e where a  $90^\circ$  zero-phase wavelet is used, one can see that the portions of the wavelets in the box resemble that of the sine waves in the box in Figure 2a. Hence, for opposite polarity, equation (3) gives results that are comparable to an input  $90^\circ$ -phase wavelet, not an input zero-phase wavelet.

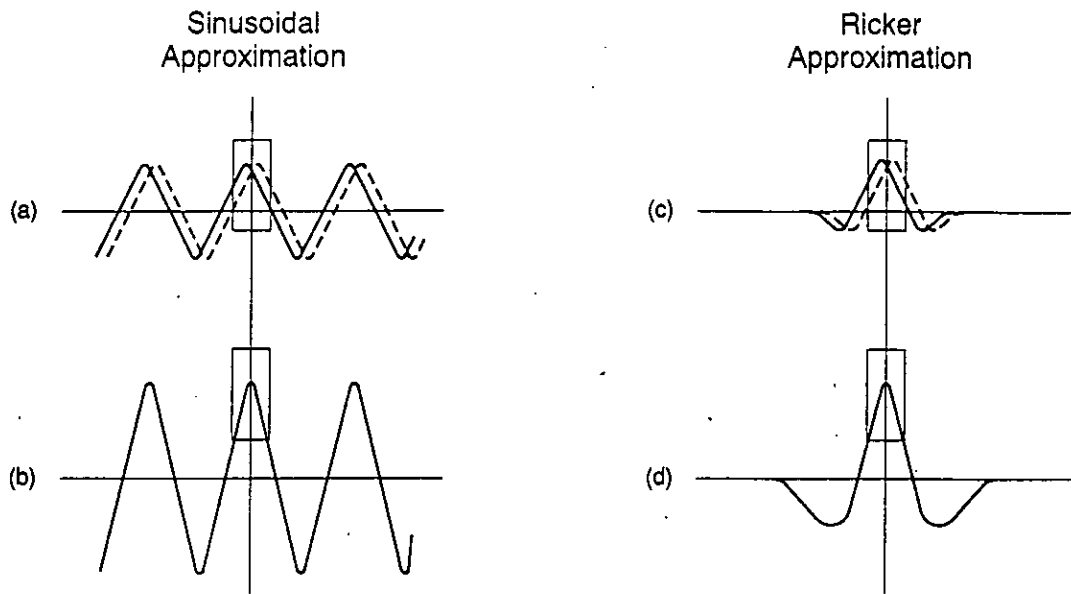


FIG. 1. Sinusoidal and Ricker Approximations for equal polarity.

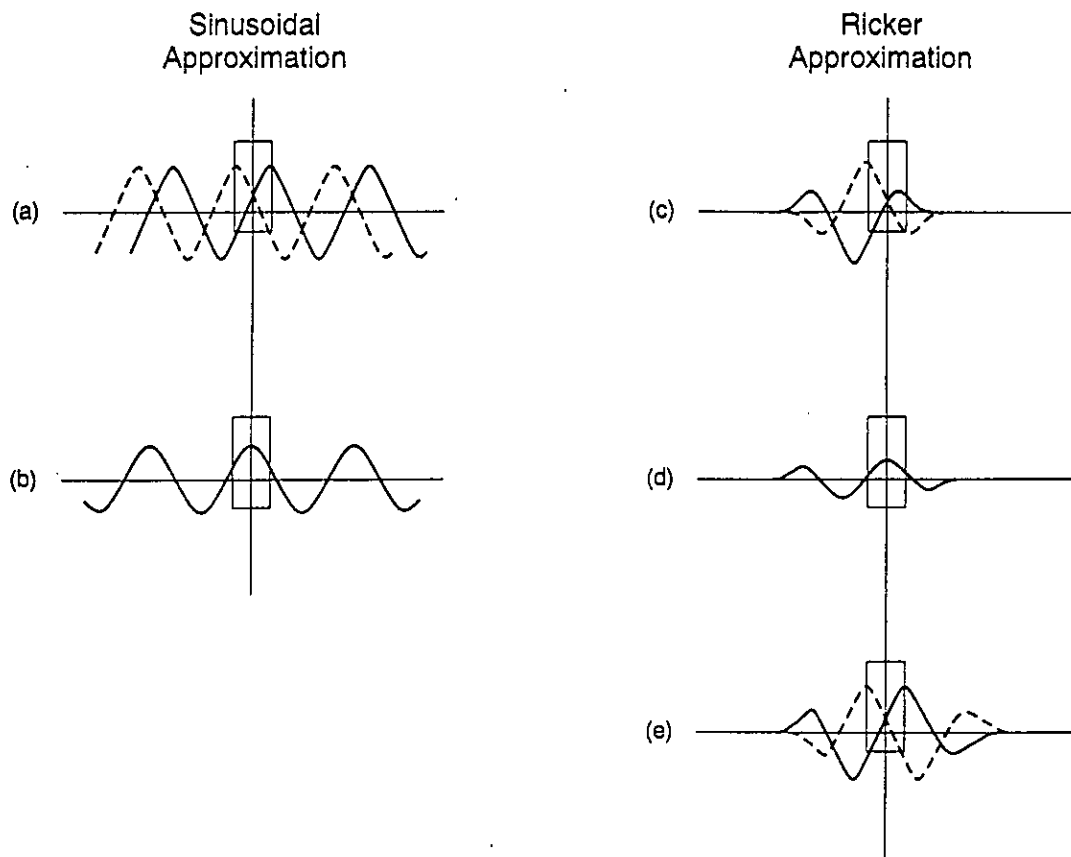


FIG. 2. Sinusoidal and Ricker Approximations for opposite polarity.

Figures 1 and 2 also explain two observations about equation (3). As will be shown later, the rate of change of the amplitude as a function of thickness in the thickness of interest is larger for opposite polarity than for equal polarity. The reason is that for opposite polarity, the maximum amplitude of the reflected composite wavelet comes from the summation of the sine curves around the halfway point between a peak and a trough where the gradients of the curves are maximum. On the contrary, for equal polarity the corresponding maximum amplitude comes from the summation around the peak of the sine waves where the gradient is around zero, resulting in a slower change in amplitude as the thickness varies.

The second observation is that, in Widess' paper (1973), the  $A_1$  in equation (3) is assumed to be the mean of the input wavelet absolute peak and trough amplitudes, instead of the absolute peak amplitude. However, he did not elaborate on the reason for this assumption. Figure 2c explains it succinctly. In practice, if we want to use a zero-phase wavelet in modelling as an input wavelet for the opposite-polarity case, the maximum amplitude of the reflected composite wavelet will always be lower than those calculated from equation (3) by a factor dependent on the functional form of the wavelet for reasons shown in Figure 2c. However, we can use equation (8) which is derived specifically for an input Ricker zero-phase wavelet for the Widess case. We shall discuss this in more detail in the next section.

Finally, it should be emphasized that a significant attribute of equation (3) is that, given any two-spikes reflectivity series, it predicts the behavior of the amplitude as a function of thickness for a thin bed situation, and there is no inherent restriction on the exact functional form of the input wavelet.

### Ricker Zero-Phase Wavelet

For a Ricker zero-phase wavelet, whose analytical expression is known, one can derive amplitude equations similar to equation (3) for the case of  $r_1 = -r_2$  and  $r_1 = r_2$ . For  $|r_1| \neq |r_2|$ , because of the complication in the mathematics, one cannot directly derive an amplitude equation similar to equation (3). However, as will be shown later, one can indirectly derive a similar equation for this general situation. We shall discuss this in more detail later.

Let us now consider the Widess' case, i.e. equal-magnitude and opposite-polarity spikes. One can derive an expression similar to equation (3) (with  $r_1 = -r_2$ ) by using the analytical expression for a Ricker zero-phase wavelet, which is one of the most commonly used wavelets in modelling. We will first derive this expression and then compare it to equation (3). The comparison will shed some light on the validity of the sinusoidal assumption, at least in the case of a Ricker zero-phase wavelet.

In the time domain, a Ricker zero-phase wavelet with the peak at  $t = 0$  is given by:

$$X(t) = A_i (1 - 2\pi^2 f_o^2 t^2) e^{-\pi^2 f_o^2 t^2} \quad (4)$$

where  $f_o$  = the peak frequency and  $A_i$  = the maximum peak amplitude

Consider two reflection spikes of opposite-polarity and equal amplitude  $r$  and separated by  $2\Delta t$ . Choosing the centre between the two spikes as reference zero time, the convolution of the Ricker zero-phase wavelet with this reflectivity series can be written as:

$$R(t) = A_i r \left[ 1 - 2\pi^2 f_o^2 (t - \Delta t)^2 \right] e^{-\pi^2 f_o^2 (t - \Delta t)^2} - A_i r \left[ 1 - 2\pi^2 f_o^2 (t + \Delta t)^2 \right] e^{-\pi^2 f_o^2 (t + \Delta t)^2}$$

For a thin bed,  $\Delta t$  is very small. Ignoring terms of second order in  $\Delta t$ , we have:

$$R(t) = A_i r e^{-\pi^2 f_o^2 t^2} \left\{ \left[ 1 - 2\pi^2 f_o^2 (t^2 - 2t\Delta t) \right] e^{\pi^2 f_o^2 2t\Delta t} - \left[ 1 - 2\pi^2 f_o^2 (t^2 + 2t\Delta t) \right] e^{-\pi^2 f_o^2 2t\Delta t} \right\}$$

Expanding the exponential terms within the brackets on the right-hand side and ignoring terms of second order in  $\Delta t$ , we obtain:

$$R(t) = A_i r e^{-\pi^2 f_o^2 t^2} \left\{ \left[ 1 - 2\pi^2 f_o^2 (t^2 - 2t\Delta t) \right] \left[ 1 + 2\pi^2 f_o^2 t\Delta t \right] - \left[ 1 - 2\pi^2 f_o^2 (t^2 + 2t\Delta t) \right] \left[ 1 - 2\pi^2 f_o^2 t\Delta t \right] \right\}$$

Expanding the terms within the brackets and ignoring terms of second order in  $\Delta t$ , we have:

$$\begin{aligned} R(t) &= A_i r e^{-\pi^2 f_o^2 t^2} \left\{ 12\pi^2 f_o^2 t\Delta t - 8\pi^4 f_o^4 t^3 \Delta t \right\} \\ &= A_i r 4\pi^2 f_o^2 \Delta t e^{-\pi^2 f_o^2 t^2} \left\{ 3t - 2\pi^2 f_o^2 t^3 \right\} \end{aligned} \quad (5)$$

For maximum or minimum  $R(t)$ :

$$\frac{dR(t)}{dt} = 0 = A_i r 4\pi^2 f_o^2 \Delta t \left[ -2\pi^2 f_o^2 e^{-\pi^2 f_o^2 t^2} (3t - 2\pi^2 f_o^2 t^3) + e^{-\pi^2 f_o^2 t^2} (3 - 6\pi^2 f_o^2 t^2) \right]$$

Simplifying, we have:

$$4\pi^4 f_o^4 t^4 - 12\pi^2 f_o^2 t^2 + 3 = 0$$

$$\therefore t^2 = \frac{12\pi^2 f_o^2 \pm \sqrt{144\pi^4 f_o^4 - 48\pi^4 f_o^4}}{8\pi^4 f_o^4}$$



$$= \frac{12 \pm \sqrt{96}}{8\pi^2 f_o^2} = \frac{3 \pm \sqrt{6}}{2\pi^2 f_o^2}$$

$$\therefore t = \pm \left( \frac{3 \pm \sqrt{6}}{2} \right)^{\frac{1}{2}} \frac{1}{\pi f_o} \quad (6)$$

Equation (6) shows that there are four roots for  $t$ , implying the existence of a total of four peaks and/or troughs for the reflected composite wavelet. This is in agreement with the fact that the reflected composite wavelet is a Ricker 90°-phase wavelet and has two peaks and two troughs, as shown in Figure 2c. Since we are interested in the absolute maximum amplitude, we will only consider the root that corresponds to a higher-amplitude peak or trough with a positive  $t$  value.

$$\therefore t = \left( \frac{3 - \sqrt{6}}{2} \right)^{\frac{1}{2}} \frac{1}{\pi f_o} = \frac{0.5246}{\pi f_o}$$

$$= \frac{K}{\pi f_o} \text{ where } K = 0.5246$$

Substituting this  $t$  value into equation (5), we get:

$$R(t) = A_i r 4\pi^2 f_o^2 \Delta t e^{\left( -\pi^2 f_o^2 \frac{K^2}{\pi^2 f_o^2} \right)} \left\{ \frac{3K}{\pi f_o} - \frac{2\pi^2 f_o^2 K^3}{\pi f_o} \right\}$$

$$= A_i r 4\pi f_o e^{-K^2} \Delta t (3K - 2K^3)$$

$$= 4\pi A_i r \Delta t f_o M \quad (7)$$

where  $M = e^{-K^2} (3K - 2K^3) = 0.9759$

Note that  $\Delta t f_o = \frac{b}{V} f_o = \frac{b}{\lambda_o}$  where  $b$  is the thickness of the bed, and  $V$  is the P-wave velocity in the bed. Note also that  $f_o$  and  $\lambda_o$  are the peak frequency and peak wavelength respectively. As shown by Kalweit and Wood (1982), they are related to the predominant frequency  $f_d$  and the predominant wavelength  $\lambda_d$  by the following relations:

$$f_d = 1.3 f_o \quad \text{and} \quad \lambda_d = \frac{1}{1.3} \lambda_o$$

Using the above relations, equation (7) can be rewritten as:

$$\begin{aligned} R(t) &= \frac{4\lambda A_i r b M}{1.3 \lambda_d} = \frac{0.9759}{1.3} \left( \frac{4\pi A_i r b}{\lambda_d} \right) \\ &= 0.75 \left( \frac{4\pi A_i r b}{\lambda_d} \right) \end{aligned} \quad (8)$$

Equation (8) gives the absolute maximum amplitude for the reflected composite wavelet from two reflection spikes of opposite polarity and equal magnitude with a Ricker zero-phase wavelet as an input wavelet. Let us compare equation (8) with Widess' amplitude expression, i.e. equation (a). In equation (8), on the right-hand side, the term within the bracket is, in fact, Widess' amplitude expression. Hence, the two expressions have the same functional form and differ only by a constant. Note that in Widess' expression, because of the problem explained in Figure 2,  $A_i$  is not the maximum peak amplitude of the input wavelet that the sine wave approximates, but is that maximum peak amplitude modified by a constant factor. Comparison to equation (8) indicates that the constant factor is 0.75 if the input wavelet is a Ricker zero-phase wavelet.

Let us now consider the case of two equal-polarity and equal-magnitude reflection spikes separated by  $2\Delta t$ . If we convolve a Ricker zero-phase wavelet with this reflectivity series, choosing the centre of the two spikes as zero reference time, the composite wavelet can be written as:

$$R(t) = A_i r \left[ 1 - 2\pi^2 f_o^2 (t - \Delta t)^2 \right] e^{-\pi^2 f_o^2 (t - \Delta t)^2} + A_i r \left[ 1 - 2\pi^2 f_o^2 (t + \Delta t)^2 \right] e^{-\pi^2 f_o^2 (t + \Delta t)^2}$$

where  $A_i$  = maximum peak amplitude of input wavelet and  $r$  = magnitude of the reflection spikes.

From symmetry, the maximum peak of the composite wavelet occurs at  $t = 0$ . Hence, if  $A_r$  is the maximum amplitude of the peak, we have:

$$\begin{aligned} A_r &= A_i r \left( 1 - 2\pi^2 f_o^2 \Delta t^2 \right) e^{-\pi^2 f_o^2 \Delta t^2} + A_i r \left( 1 - 2\pi^2 f_o^2 \Delta t^2 \right) e^{-\pi^2 f_o^2 \Delta t^2} \\ &= 2A_i r \left( 1 - 2\pi^2 f_o^2 \Delta t^2 \right) e^{-\pi^2 f_o^2 \Delta t^2} \\ &= 2A_i r \left( 1 - 2\pi^2 f_o^2 \Delta t^2 \right) \left( 1 - \pi^2 f_o^2 \Delta t^2 \right), \text{ ignoring terms of } O(t^4) \text{ and higher for small } \Delta t. \end{aligned}$$

From the above expression, it is evident that, unlike for the case of equal-magnitude and opposite-polarity spikes, terms of second order in  $\Delta t$  cannot be ignored. This is probably due to the fact that, as mentioned earlier, the rate of change of amplitude as a function of thickness is much smaller for the equal-polarity spikes than for the opposite-polarity spikes. Hence, higher order of  $\Delta t$  is needed for the equal-polarity spikes to differentiate different amplitudes for small thickness range. Rewriting the expression for  $A_r$ , we have:

$$\begin{aligned}
 A_r &= 2A_i r \left[ 1 - 3\pi^2 f_o^2 \Delta t^2 \right], \text{ ignoring terms of } O(\Delta t^4) \\
 &= 2A_i r \left[ 1 - 3 \left( \frac{\pi b}{1.3\lambda_d} \right)^2 \right] \\
 &= 2A_i r \left[ 1 - 1.775 \left( \frac{\pi b}{\lambda_d} \right)^2 \right] \tag{9}
 \end{aligned}$$

Equation (9) is the expression sought. It gives the maximum peak amplitude for the composite wavelet resulting from the convolution of a Ricker zero-phase wavelet with a two-spikes reflectivity series of equal magnitude and equal polarity. It can be rewritten as:

$$A_r = 2A_i r \left[ 1 - 2 \left( \frac{\pi b}{\lambda_d} \right)^2 \right] + 0.45A_i r \left( \frac{\pi b}{\lambda_d} \right)^2 \tag{10}$$

The first term in the right-hand side of equation (10) is exactly the same as the  $A_r$  given by equation (3) by putting  $r_1 = r_2$ . Thus, using a sinusoidal approximation for a Ricker zero-phase wavelet for the case of equal-magnitude and equal-polarity will

introduce an error of a decrease of  $0.45A_i r \left( \frac{\pi b}{\lambda_d} \right)^2$  in the peak amplitude. This error is a function of the bed thickness. Table 1 shows the percentage error between the two methods as a function of thickness calculated as follows:

$$\% \text{ error} = \frac{0.45A_i r \left( \frac{\pi b}{\lambda_d} \right)^2}{2A_i r \left[ 1 - 2 \left( \frac{\pi b}{\lambda_d} \right)^2 \right]} \times 100\%$$

From Table 1, it is evident that the sinusoidal approximation is a good approximation for the Ricker zero-phase wavelet for the equal-magnitude and equal-polarity thin bed if its thickness is less than 1/8 of the predominant wavelength, assuming one accepts a 10% difference as the limit of acceptable deviation. Below that thickness, the differences are fairly small. It is interesting to note that the percentage error increases sharply beyond the  $(1/8)\lambda_d$  thickness.

Table 1 % Error for Sinusoidal Approximation

| $b / \lambda_d$ | % error |
|-----------------|---------|
| 1/20            | 1.2     |
| 1/18            | 1.5     |
| 1/16            | 1.9     |
| 1/14            | 2.5     |
| 1/12            | 3.6     |
| 1/10            | 5.5     |
| 1/8             | 10.0    |
| 1/6             | 27.3    |

Unfortunately, the complicated mathematics involved inhibits the direct derivation of a simple expression equivalent to equations (8) and (9) for the general case of two reflection spikes where  $|r_1| \neq |r_2|$ . However, one can derive an expression for the general case in the following manner. Consider firstly the case of two reflection spikes having different magnitudes and are of opposite polarities. We can decompose the two spikes as follows:

$$-r_1 \uparrow \uparrow r_2 = -r_3 \uparrow \uparrow r_3 + \begin{cases} r_4 \uparrow \uparrow r_4, & r_1 < r_2 \\ -r_4 \uparrow \uparrow -r_4, & r_1 > r_2 \end{cases} \quad (11)$$

where  $r_3 = \frac{r_1 + r_2}{2}$  and  $r_4 = \frac{-r_1 + r_2}{2}$ . In other words, the different-magnitude and opposite-polarity spikes have been decomposed into the sum of an equal-magnitude and opposite-polarity term and an equal-magnitude and equal-polarity term. Similarly, we can do the same for two spikes having different magnitude and are of equal polarities:

$$r_5 \quad | \quad r_6 = -r_7 \quad | \quad r_8 \quad (12)$$

where  $r_7 = \frac{-r_5 + r_6}{2}$  and  $r_8 = \frac{r_5 + r_6}{2}$

Since convolution is linear, the convolutions of a wavelet with the left-hand sides of equations (11) and (12) are equal to the convolutions of the same wavelet with the right-hand sides. It is then evident that, for the general situation of  $|r_1| \neq |r_2|$ , the amplitude equation is simply the sum of equations (8) and (9). For example, consider equation (11), we can write:

$$A_o = A_i \left\{ (2r_4)^2 \left[ 1 - 1.775 \left( \frac{\pi b}{\lambda_d} \right)^2 \right]^2 + 0.75^2 (2r_3)^2 \left( \frac{2\pi b}{\lambda_d} \right)^2 \right\}^{\frac{1}{2}}$$

$$= A_i \left\{ (-r_1 + r_2)^2 \left[ 1 - 1.775 \left( \frac{\pi b}{\lambda_d} \right)^2 \right]^2 + 0.75^2 (r_1 + r_2)^2 \left( \frac{2\pi b}{\lambda_d} \right)^2 \right\}^{\frac{1}{2}} \quad (13)$$

Note that we will use  $A_o$  and  $A_i$  to represent the absolute maximum amplitudes of the reflected composite wavelets for Ricker approximation and sinusoidal approximation respectively.

However, compared to equation (3) where the signs associated with the reflection spikes are embedded, here the signs are explicitly written out to facilitate the decompositions. In other words, in equation (3),  $r_1$  and  $r_2$  can be negative or positive numbers, and in equation (13),  $r_1$  and  $r_2$  are the magnitudes of the reflection spikes and are positive numbers. Thus, to be consistent with equation (3), equation (13) should be re-written as:

$$A_o = A_i \left\{ (r_1 + r_2)^2 \left[ 1 - 1.775 \left( \frac{\pi b}{\lambda_d} \right)^2 \right]^2 + 0.75^2 (r_2 - r_1)^2 \left( \frac{2\pi b}{\lambda_d} \right)^2 \right\}^{\frac{1}{2}} \quad (14)$$

where  $r_1$  and  $r_2$  have embedded signs.

Similarly, one can show that equation (14) also works for the case represented by equation (12).

From the foregoing discussion, equation (3) can now be rewritten as:

$$A_r = A_i \left\{ (r_1 + r_2)^2 \left[ 1 - 2 \left( \frac{\pi b}{\lambda_d} \right)^2 \right]^2 + M^2 (r_2 - r_1)^2 \left( \frac{2\pi b}{\lambda_d} \right)^2 \right\}^{\frac{1}{2}} \quad (15)$$

where  $M$  is a constant to rectify the problem explained in Figures 1 and 2, and its value is dependent on the functional form of the input wavelet. We have shown that for equal-polarity spikes,  $M$  is 1. For opposite-polarity spikes,  $M$  is 1 for a Ricker 90°-phase input wavelet, and is 0.75 if the wavelet is zero-phase.

In the next section, the results from modelling will be plotted and compared with the results from equations (14) and (15) to determine if they are valid.

### Vertical Incidence, Single Layer

In this section, we will compare the results from equations (14) and (15) with the results from numerical modelling for vertically-incident plane waves. To study the amplitude response of a thin bed to vertically-incident plane waves, a simple wedge model (Figure 3) is used. Its geometry is set up so that the trace numbers in the resulting synthetic seismograms are equal to the thicknesses of the wedge in metres, that is, trace 1

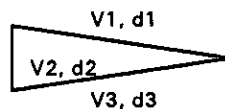


FIG. 3 A Wedge Model

corresponds to a thickness of 1 metre, trace 2 2 metres, etc. Because of the thickness of interest, the number of traces plotted for each synthetic seismogram will only cover two to four metres more than the  $(1/4)\lambda_d$  thickness. Since different models have different velocities for the thin beds, the number of traces plotted for various synthetic seismograms will be different, depending on the models and the peak frequencies of the input wavelets. Unless specified otherwise, all synthetic seismograms are generated by convolving a 31 Hz (peak frequency) zero-phase Ricker wavelets with two-spikes reflectivity series, since 31 Hz is a rather common peak frequency on seismic data from Western Canada. Other peak frequencies will also be used to test the frequency dependency of the equations. A 90°-phase wavelet will also be used whenever is appropriate. Note that, however, based on the second moments of wavelets, Berkout (1984) showed that a zero-phase wavelet gives the maximum vertical resolution compared to other phases. For reasons mentioned earlier, transmission loss and internal multiples are ignored, and all models are run at 0.1 ms sampling rate. The maximum peak amplitude of any input Ricker wavelet is set at 1000.

Six different two-terms reflectivity series will be studied:

- (a)  $\top\perp$  opposite polarity and equal magnitude (model 1A)
- (b)  $\perp\perp$  opposite polarity and unequal magnitude (model 1B)
- (c)  $\top\top$  opposite polarity and unequal magnitude (model 1C)
- (d)  $\perp\perp$  equal polarity and equal magnitude (model 1D)
- (e)  $\perp\perp$  equal polarity and unequal magnitude (model 1E)
- (f)  $\perp\perp$  equal polarity and unequal magnitude (model 1F)

The densities and velocities used for the various models are listed in Table 2. Note that for all the six models, the reflection coefficients for the upper interface and lower interface are referred to as  $r_1$  and  $r_2$  respectively. They are chosen to reflect the general situation in the early Cretaceous formations in Southern Alberta. Figures 4a to 4f show the synthetic seismograms for the six models.

### Opposite Polarity and Equal Magnitude

This case is referred to as model 1A. It represents the situation of a thin bed embedded in a homogeneous and isotropic medium so thick that there is no interference effect from the overlying and underlying strata. Although such a bed is rarely encountered in real geological situations, it is the most studied case in thin-bed interpretation because of its simplicity. Since  $r_1 = -r_2 = 0.2072$ , equations (14) and (15) reduce to:

$$A_0 = 0.75 \left( \frac{4\pi A_i r b}{\lambda_d} \right) \text{ where } r = |r_1| = |r_2| \text{ and } A_r = M \left( \frac{4\pi A_i r b}{\lambda_d} \right) \text{ respectively.}$$

Recall that  $A_0$  corresponds to Ricker zero-phase wavelet approximation and  $A_r$  corresponds to sinusoidal approximation as discussed in the last section. For a Ricker input wavelet,  $M$  is 1 if it is 90°-phase, and is 0.75 if it is zero-phase. Furthermore, according to the derivation,  $M$  is a constant independent of frequency. To check these properties of  $M$ , model 1A is run six times with six different Ricker wavelets, three zero-phase wavelets at 18 Hz, 31 Hz and 50 Hz peak frequencies, and three 90°-phase wavelets at the same frequencies. The results are listed in Tables 3a, 3b and 3c, and they are plotted in Figs. 5a, 5b and 5c.

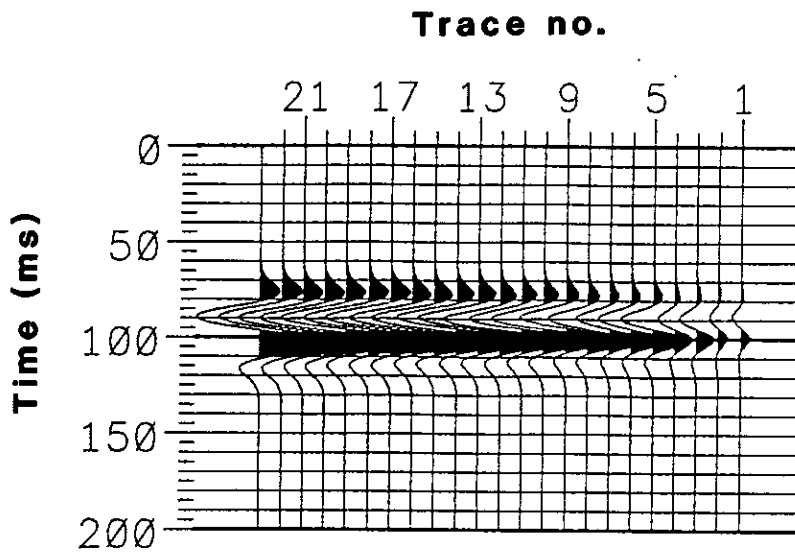


FIG. 4a Synthetic seismogram for model 1A.

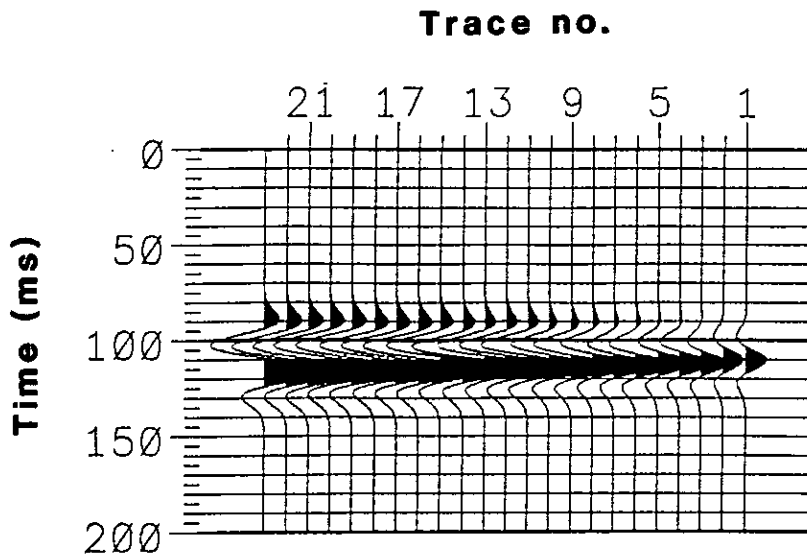


FIG. 4b Synthetic seismogram for model 1B.



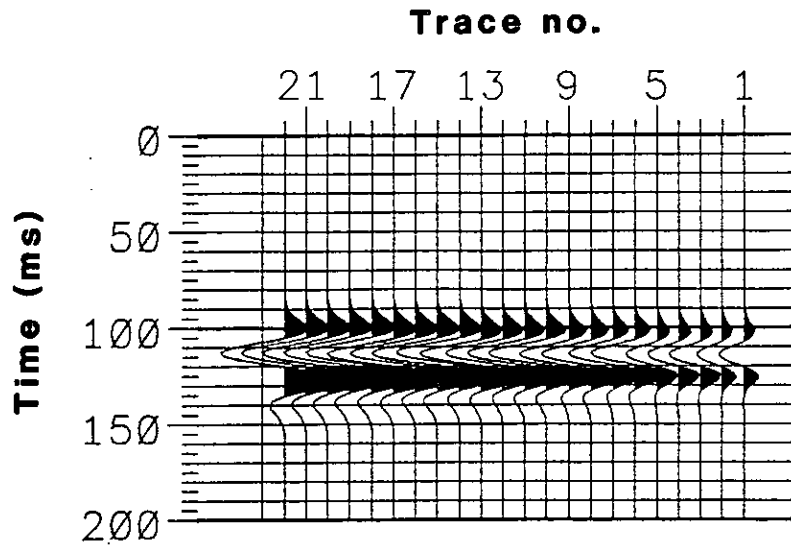


FIG. 4c Synthetic seismogram for model 1C.

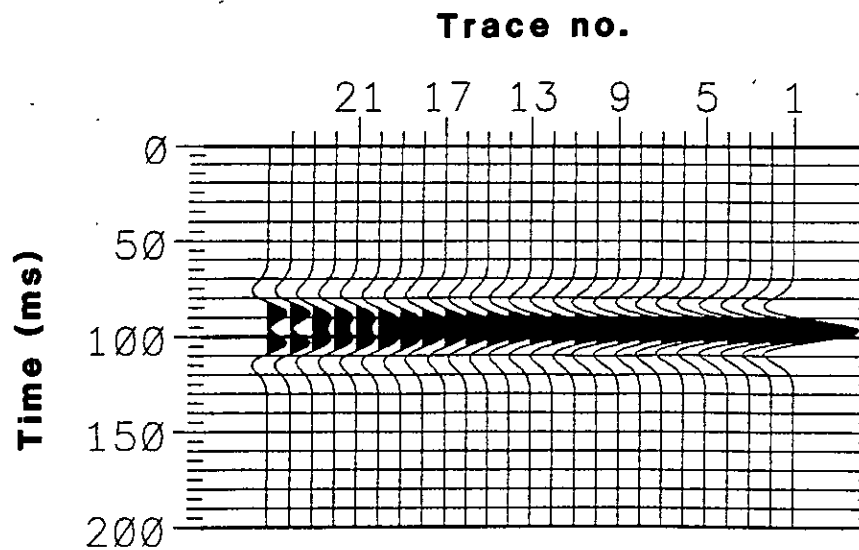


FIG. 4d Synthetic seismogram for model 1D.

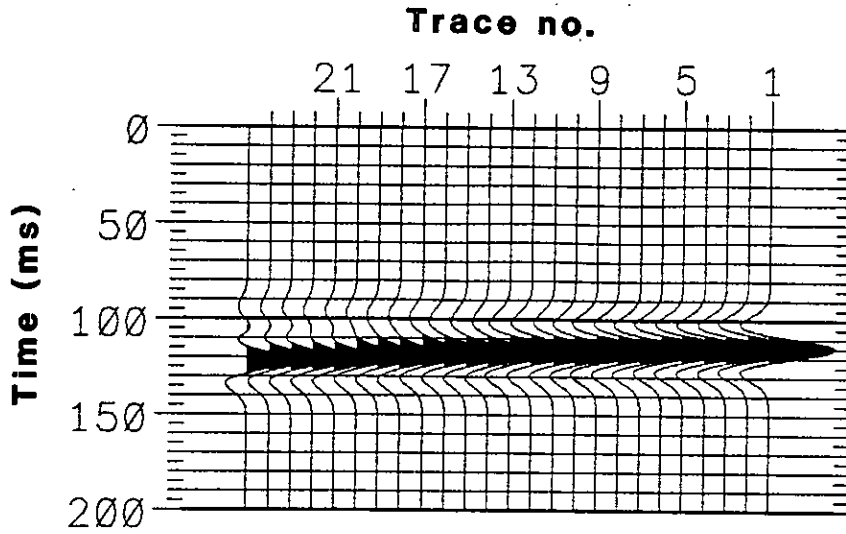


FIG. 4e Synthetic seismogram for model 1E.

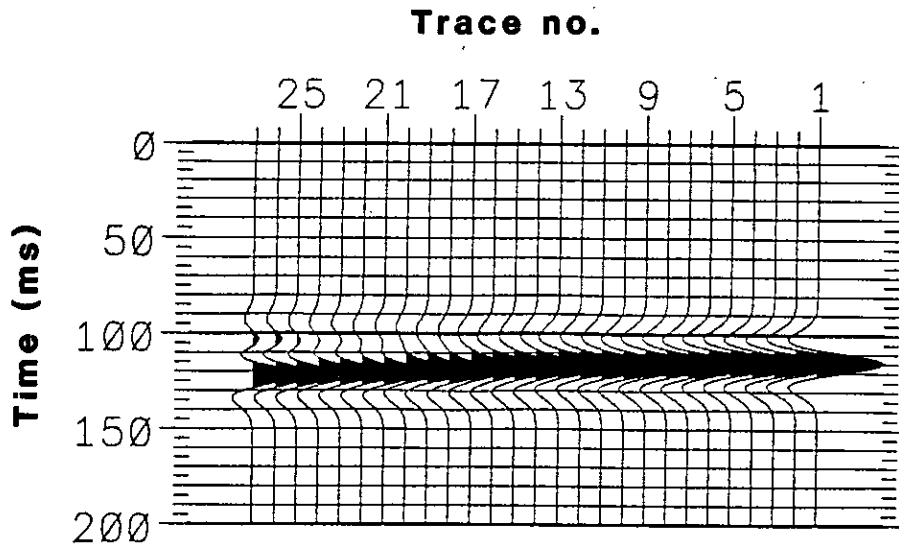


FIG. 4f Synthetic seismogram for model 1F.

Table 2 Lithology, Layer Velocities, Layer Densities, and Reflection Coefficients for Six Models

| Model | Lithology Modelled      |         | Lithology Modelled  |         | Lithology Modelled      |         | $r_1$   | $r_2$  |
|-------|-------------------------|---------|---------------------|---------|-------------------------|---------|---------|--------|
|       | V1 (m/s)                | d(g/cc) | V2 (m/s)            | d(g/cc) | V3 (m/s)                | d(g/cc) |         |        |
| 1A    | non-porous sand<br>4267 | 2.505   | porous sand<br>3048 | 2.303   | non-porous sand<br>4267 | 2.505   | -0.2072 | 0.2072 |
| 1B    | silt<br>3800            | 2.434   | porous sand<br>3048 | 2.303   | non-porous sand<br>4267 | 2.505   | -0.1371 | 0.2072 |
| 1C    | non-porous sand<br>4267 | 2.505   | porous sand<br>3048 | 2.303   | silt<br>3800            | 2.434   | -0.2072 | 0.1371 |
| 1D    | porous sand<br>3048     | 2.303   | silt<br>3560        | 2.434   | non-porous sand<br>4267 | 2.505   | 0.1047  | 0.1047 |
| 1E    | porous sand<br>3048     | 2.303   | shale<br>3353       | 2.359   | non-porous sand<br>4267 | 2.505   | 0.0596  | 0.1494 |
| 1F    | porous sand<br>3048     | 2.303   | silt<br>3800        | 2.434   | non-porous sand<br>4267 | 2.505   | 0.1371  | 0.0722 |

Note that in both Table 3 and Fig. 4, the Ricker and sinusoidal approximations are only listed and plotted to a thickness slightly beyond the  $(1/8)\lambda_d$  value. This is because these approximations are not expected to be valid beyond this thickness, if one accepts a 10% difference as the limit of good agreement between these approximations and the modelling data, as mentioned in the last section. As Table 3 indicates, the percentage differences between the modelling data and the sinusoidal and Ricker approximations are less than 10% for thicknesses less than the  $(1/8)\lambda_d$  value. For thicknesses below  $(1/16)\lambda_d$ , the fluctuations in the percentage differences reflect somewhat the non-systematic round-off errors resulting from using a discrete sampling rate in modelling. As the thickness increases to beyond the  $(1/16)\lambda_d$  value, the percentage difference begins to increase steadily, reflecting the fact that bed is getting thicker, and the thin-bed assumption is slowly being violated. The modelling values are listed and plotted to a thickness slightly beyond the  $(1/4)\lambda_d$  value, since our thickness of interest is up to  $(1/4)\lambda_d$  value. As shown in Figs. 5a, 5b and 5c, tuning occurs at about  $(1/4)\lambda_d$  thickness, which is a well-known effect and needs no further comment.

In Table 3, the amplitude values for the Ricker approximation are obtained by multiplying the corresponding amplitudes for sinusoidal approximation by 0.75. The results agree well with the modelling results with Ricker zero-phase wavelet as input for up to about  $(1/8)\lambda_d$  thickness for all three frequencies. This implies that the Ricker zero-phase approximation is correct and that  $M$  is indeed independent of frequencies. However, Fig. 4 shows an interesting property of the Ricker zero-phase approximation. Notice that the modelling curve with zero-phase wavelet input deviates from the Ricker zero-phase approximation faster than that with the  $90^\circ$ -phase wavelet input from the sinusoidal approximation for all three frequencies. The reason is probably due to ignoring second and higher order terms in  $\Delta t$  when the expression  $A_0$  is derived for the case of  $r_2 = -r_1$ . As explained in the last section, second order term in  $\Delta t$  is actually needed if the summing of wavelets involves the region around the peak or trough area of the wavelet. Fig. 2c clearly shows that the summing of a Ricker zero-phase wavelet with its reverse separated by  $\Delta t$  would involve the side trough of the wavelet.

Based on the results shown in Table 3 and Fig. 5, one can conclude that both the sinusoidal and Ricker zero-phase approximation are good approximations for beds that are below the  $(1/8)\lambda_d$  thickness, and are independent of frequencies. In practice, the existence of a constant  $M$  in the sinusoidal approximation implies that, even if there is a geological situation which can be represented by model 1A, one cannot calibrate the thickness according to the amplitudes observed on real seismic data unless the wavelet is known, or the data ties with at least one well for the target formation. If there is no well tie, one may try to extract a wavelet from the data; if it approximates a Ricker zero-phase wavelet, then  $M$  is roughly 0.75. If the wavelet does not approximate a Ricker zero-phase wavelet, one might be able to estimate  $M$  by modelling with the extracted wavelet as an input wavelet.

Table 3a Comparison of Modelling Data with Ricker and Sinusoidal Approximations for Model 1A at 18 Hz Peak Frequency ( $\lambda_p = 130.26$  m)

| Thickness<br>(m) | $(t/\lambda_p) \times 10^{-1}$ | Absolute Maximum Amplitude (Input = 1000) |                  |                              |                         |                  |                              |
|------------------|--------------------------------|---|------------------|------------------------------|-------------------------|------------------|------------------------------|
|                  |                                | Zero-Phase Input Wavelet                  |                  |                              | 90°-Phase Input Wavelet |                  |                              |
|                  |                                | Ricker<br>(R)                             | Modelling<br>(M) | $\frac{R-M}{R} \times 100\%$ | Sinusoidal<br>(S)       | Modelling<br>(M) | $\frac{S-M}{S} \times 100\%$ |
| 0                | 0.00                           | 0.00                                      | 0.00             | 0.00                         | 0.00                    | 0.00             | 0.00                         |
| 1                | 0.77                           | 15.01                                     | 16.00            | -6.60                        | 19.99                   | 19.92            | 0.35                         |
| 3                | 2.30                           | 45.03                                     | 43.28            | 3.89                         | 59.97                   | 59.56            | 0.68                         |
| 5                | 3.83                           | 75.05                                     | 74.60            | 0.60                         | 99.94                   | 100.09           | -0.15                        |
| 7                | 5.37                           | 105.07                                    | 102.85           | 2.11                         | 139.92                  | 138.10           | 1.30                         |
| 9                | 6.91                           | 135.09                                    | 130.01           | 3.76                         | 179.90                  | 181.53           | -0.91                        |
| 11               | 8.44                           | 165.11                                    | 155.80           | 5.64                         | 219.88                  | 217.54           | 1.06                         |
| 13               | 9.98                           | 195.13                                    | 179.96           | 7.77                         | 259.86                  | 251.26           | 3.31                         |
| 15               | 11.52                          | 225.15                                    | 203.90           | 9.44                         | 299.83                  | 284.66           | 5.06                         |
| 17               | 13.05                          | 255.17                                    | 222.52           | 12.80                        | 339.81                  | 310.62           | 8.59                         |
| 19               | 14.59                          | -   | 241.87           | -                            | -                       | 337.53           | -                            |
| 21               | 16.12                          | -   | 257.41           | -                            | -                       | 359.08           | -                            |
| 23               | 17.66                          | -   | 270.53           | -                            | -                       | 377.14           | -                            |
| 25               | 19.19                          | -   | 281.17           | -                            | -                       | 391.67           | -                            |
| 27               | 20.73                          | -   | 289.89           | -                            | -                       | 403.29           | -                            |
| 29               | 22.26                          | -   | 295.11           | -                            | -                       | 409.94           | -                            |
| 31               | 23.80                          | -   | 298.50           | -                            | -                       | 413.74           | -                            |
| 33               | 25.33                          | -   | 299.67           | -                            | -                       | 414.02           | -                            |
| 35               | 26.87                          | -   | 298.75           | -                            | -                       | 411.24           | -                            |
| 37               | 28.40                          | -   | 295.67           | -                            | -                       | 404.66           | -                            |

Table 3b Comparison of Modelling Data with Ricker and Sinusoidal Approximations for Model 1A at 31 Hz Peak Frequency ( $\lambda_p = 75.63$  m)

| Thickness (m) | $(t/\lambda_p) \times 10^{-2}$ | Absolute Maximum Amplitude (Input = 1000) |               |                              |                         |               |                              |
|---------------|--------------------------------|---|---------------|------------------------------|-------------------------|---------------|------------------------------|
|               |                                | Zero-Phase Input Wavelet                  |               |                              | 90°-Phase Input Wavelet |               |                              |
|               |                                | Ricker (R)                                | Modelling (M) | $\frac{R-M}{R} \times 100\%$ | Sinusoidal (S)          | Modelling (M) | $\frac{S-M}{S} \times 100\%$ |
| 0             | 0.00                           | 0.00                                      | 0.00          | 0.00                         | 0.00                    | 0.00          | 0.00                         |
| 1             | 1.32                           | 25.82                                     | 27.53         | -6.62                        | 34.43                   | 35.66         | -3.57                        |
| 3             | 3.97                           | 77.46                                     | 73.98         | 4.49                         | 103.28                  | 103.40        | -0.12                        |
| 5             | 6.61                           | 129.11                                    | 125.57        | 2.74                         | 172.14                  | 175.50        | -1.95                        |
| 7             | 9.26                           | 180.74                                    | 169.43        | 6.26                         | 240.99                  | 236.80        | 1.74                         |
| 9             | 11.90                          | 232.39                                    | 208.11        | 10.40                        | 309.85                  | 290.76        | 6.16                         |
| 11            | 14.54                          | -   | 240.58        | -                            | -                       | 336.00        | -                            |
| 13            | 17.19                          | -   | 266.16        | -                            | -                       | 371.34        | -                            |
| 15            | 19.83                          | -   | 285.57        | -                            | -                       | 397.72        | -                            |
| 17            | 22.48                          | -   | 295.51        | -                            | -                       | 410.48        | -                            |
| 19            | 25.12                          | -   | 298.82        | -                            | -                       | 414.15        | -                            |
| 21            | 27.77                          | -   | 297.06        | -                            | -                       | 407.41        | -                            |
| 23            | 30.41                          | -   | 289.38        | -                            | -                       | 391.81        | -                            |

Table 3c Comparison of Modelling Data with Ricker and Sinusoidal Approximations for Model 1A at 50 Hz Peak Frequency ( $\lambda_p = 46.89$  m)

| Thickness (m) | $(t/\lambda_p) \times 10^{-2}$ | Absolute Maximum Amplitude (Input = 1000) |               |                              |                         |               |                              |
|---------------|--------------------------------|---|---------------|------------------------------|-------------------------|---------------|------------------------------|
|               |                                | Zero-Phase Input Wavelet                  |               |                              | 90°-Phase Input Wavelet |               |                              |
|               |                                | Ricker (R)                                | Modelling (M) | $\frac{R-M}{R} \times 100\%$ | Sinusoidal (S)          | Modelling (M) | $\frac{S-M}{S} \times 100\%$ |
| 0             | 0.00                           | 0.00                                      | 0.00          | 0.00                         | 0.00                    | 0.00          | 0.00                         |
| 1             | 2.13                           | 41.65                                     | 44.29         | -6.34                        | 55.53                   | 57.50         | -3.55                        |
| 3             | 6.40                           | 124.94                                    | 117.16        | 6.22                         | 166.59                  | 163.74        | 1.71                         |
| 5             | 10.67                          | 208.24                                    | 191.62        | 7.98                         | 277.65                  | 267.77        | 3.56                         |
| 7             | 14.93                          | -   | 245.40        | -                            | -                       | 342.70        | -                            |
| 9             | 19.19                          | -   | 281.08        | -                            | -                       | 391.69        | -                            |
| 11            | 23.46                          | -   | 297.93        | -                            | -                       | 413.23        | -                            |
| 13            | 27.72                          | -   | 297.44        | -                            | -                       | 408.09        | -                            |
| 15            | 31.99                          | -   | 282.08        | -                            | -                       | 377.05        | -                            |

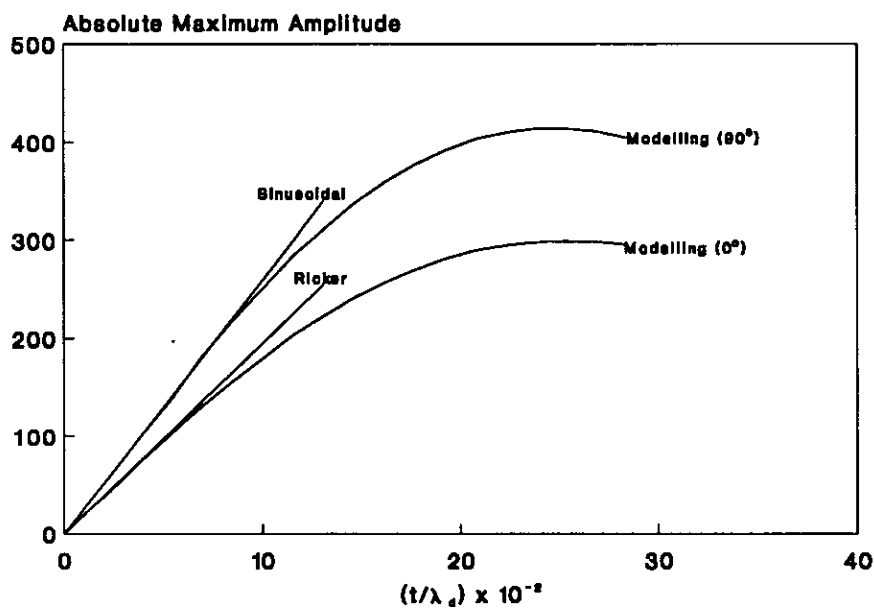


FIG. 5a The amplitude response for model 1A with Ricker 18 Hz input wavelets whose maximum amplitudes is 1000.

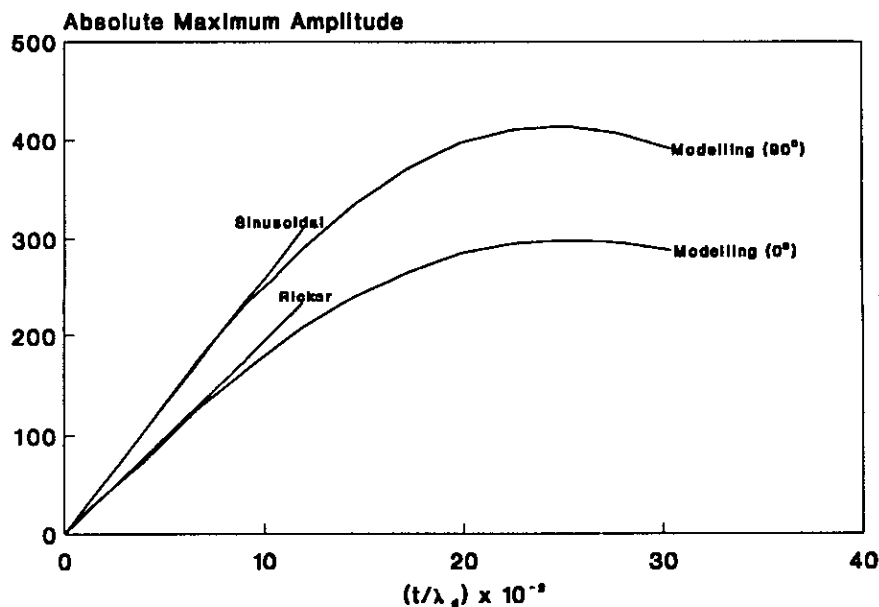


FIG. 5b The amplitude response for model 1A with Ricker 31 Hz input wavelets whose maximum amplitudes is 1000.

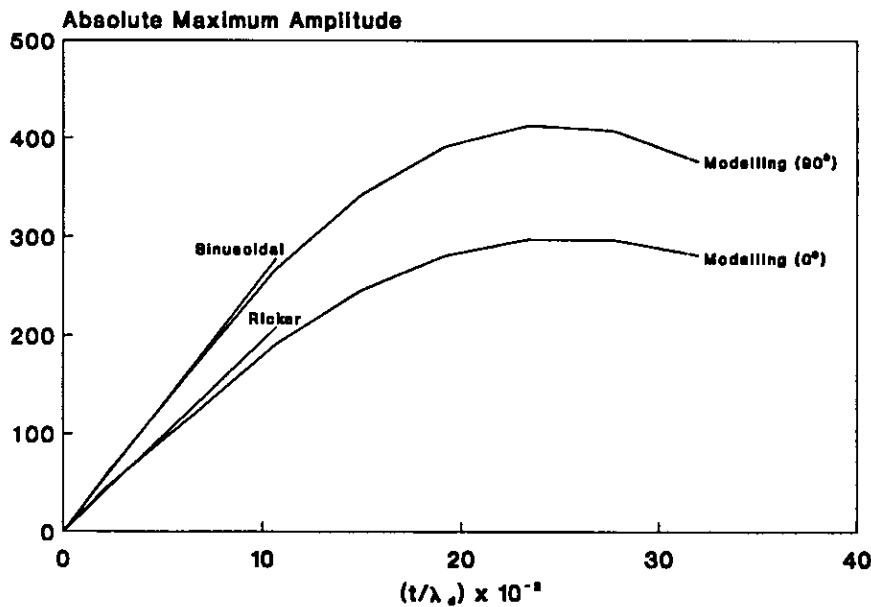


FIG. 5c The amplitude response for model 1A with Ricker 50 Hz input wavelets whose maximum amplitudes is 1000.

### Equal Polarity and Equal Magnitude

This case is referred to as model 1D. It represents the situation of a thin bed overlain by a lower-velocity half-space and underlain by a higher-velocity half-space and with the two reflection coefficients having the same magnitude. As with model 1A, such a bed is also rarely encountered in real geological situations. However, the study of it helps to understand some subtle aspects of thin-bed tuning.

$$\text{Since } r_1 = r_2, \text{ equations (2.14) and (2.15) reduce to } A_0 = 2A_1 r \left[ 1 - 1.775 \left( \frac{\pi b}{\lambda_d} \right)^2 \right]$$

$$\text{and } A_r = 2A_1 r \left[ 1 - 2 \left( \frac{\pi b}{\lambda_d} \right)^2 \right] \text{ where } r = r_1 = r_2. \text{ These two simplified expressions differ}$$

only in one of the constants within the bracket, and the resulting difference between  $A_0$  and  $A_r$  as a function of  $b$  is rather small, as shown in Table 1. To study these approximations, model 1D is run with three different Ricker zero-phase wavelets at 18 Hz, 31 Hz and 50 Hz peak frequencies. Note that for the amplitude study of model 1D, a Ricker zero-phase wavelet gives the same results as a 90°-phase wavelet, since the maximum amplitudes resulting from summing both wavelets come from similar regions around the peaks of both wavelets.



Table 4a Comparison of Modelling Data with Ricker and Sinusoidal Approximations for Model 1D at 18 Hz Peak Frequency ( $\lambda_d = 152.14$  m)

| Thickness<br>(m) | $(t/\lambda_d) \times 10^{-2}$ | Absolute Maximum Amplitude (Input = 1000) |               |                              |                   |                              |
|------------------|--------------------------------|---|---------------|------------------------------|-------------------|------------------------------|
|                  |                                | Modelling<br>(M)                          | Ricker<br>(R) | $\frac{R-M}{M} \times 100\%$ | Sinusoidal<br>(S) | $\frac{S-M}{M} \times 100\%$ |
| 0                | 0.00                           | 209.40                                    | 209.40        | 0.00                         | 209.40            | 0.00                         |
| 1                | 0.66                           | 209.22                                    | 209.24        | 0.01                         | 209.22            | 0.00                         |
| 3                | 1.97                           | 207.95                                    | 207.97        | 0.01                         | 204.79            | -0.01                        |
| 5                | 3.29                           | 205.49                                    | 205.44        | -0.02                        | 204.94            | -0.27                        |
| 7                | 4.60                           | 201.45                                    | 201.63        | -0.01                        | 200.65            | -0.40                        |
| 9                | 5.92                           | 197.06                                    | 196.56        | -0.25                        | 194.94            | -1.09                        |
| 11               | 7.23                           | 190.59                                    | 190.22        | -0.19                        | 187.79            | -1.49                        |
| 13               | 8.54                           | 183.57                                    | 182.62        | -0.52                        | 179.22            | -2.43                        |
| 15               | 9.86                           | 175.59                                    | 173.74        | -1.06                        | 169.22            | -3.76                        |
| 17               | 11.17                          | 165.87                                    | 163.60        | -1.39                        | 157.79            | -5.12                        |
| 19               | 12.49                          | 156.11                                    | 152.19        | -2.58                        | 144.94            | -7.71                        |
| 21               | 13.80                          | 145.64                                    | 139.51        | -4.39                        | 130.65            | -11.47                       |
| 23               | 15.12                          | 134.52                                    | 125.56        | -7.14                        | -                 | -                            |
| 25               | 16.43                          | 121.85                                    | 110.35        | -10.42                       | -                 | -                            |
| 27               | 17.75                          | 110.89                                    | -             | -                            | -                 | -                            |
| 29               | 19.06                          | 97.40                                     | -             | -                            | -                 | -                            |
| 31               | 20.38                          | 83.66                                     | -             | -                            | -                 | -                            |
| 33               | 21.69                          | 72.12                                     | -             | -                            | -                 | -                            |
| 35               | 23.01                          | 62.28                                     | -             | -                            | -                 | -                            |
| 37               | 24.32                          | 58.67                                     | -             | -                            | -                 | -                            |
| 39               | 25.63                          | 58.03                                     | -             | -                            | -                 | -                            |
| 41               | 26.95                          | 59.48                                     | -             | -                            | -                 | -                            |
| 43               | 28.26                          | 61.96                                     | -             | -                            | -                 | -                            |

Table 4b Comparison of Modelling Data with Ricker and Sinusoidal Approximations for Model 1D at 31 Hz Peak Frequency ( $\lambda_d = 88.34$  m)

| Thickness (m) | $(t/\lambda_d) \times 10^{-2}$ | Absolute Maximum Amplitude (Input = 1000) |            |                              |                |                              |
|---------------|--------------------------------|---|------------|------------------------------|----------------|------------------------------|
|               |                                | Modelling (M)                             | Ricker (R) | $\frac{R-M}{M} \times 100\%$ | Sinusoidal (S) | $\frac{S-M}{M} \times 100\%$ |
| 0             | 0.00                           | 209.40                                    | 209.40     | 0.00                         | 209.40         | 0.00                         |
| 1             | 1.13                           | 208.87                                    | 208.93     | 0.03                         | 208.87         | 0.00                         |
| 3             | 3.40                           | 205.11                                    | 205.17     | 0.03                         | 204.63         | -0.23                        |
| 5             | 5.66                           | 197.90                                    | 197.65     | -0.13                        | 196.16         | -0.89                        |
| 7             | 7.92                           | 186.31                                    | 186.37     | -0.02                        | 183.45         | -1.56                        |
| 9             | 10.19                          | 173.95                                    | 171.33     | -1.53                        | 166.50         | -4.47                        |
| 11            | 12.45                          | 156.31                                    | 152.52     | -2.48                        | 145.31         | -7.57                        |
| 13            | 14.72                          | 137.90                                    | 129.96     | -6.11                        | 119.89         | -15.02                       |
| 15            | 16.98                          | 117.87                                    | 103.64     | -13.73                       | -              | -                            |
| 17            | 19.24                          | 94.74                                     | -          | -                            | -              | -                            |
| 19            | 21.51                          | 72.95                                     | -          | -                            | -              | -                            |
| 21            | 23.77                          | 59.78                                     | -          | -                            | -              | -                            |
| 23            | 26.04                          | 58.22                                     | -          | -                            | -              | -                            |
| 25            | 28.30                          | 62.17                                     | -          | -                            | -              | -                            |

Table 4c Comparison of Modelling Data with Ricker and Sinusoidal Approximations for Model 1D at 50 Hz Peak Frequency ( $\lambda_d = 54.77$  m)

| Thickness (m) | $(t/\lambda_d) \times 10^{-2}$ | Absolute Maximum Amplitude (Input = 1000) |            |                              |                |                              |
|---------------|--------------------------------|---|------------|------------------------------|----------------|------------------------------|
|               |                                | Modelling (M)                             | Ricker (R) | $\frac{R-M}{M} \times 100\%$ | Sinusoidal (S) | $\frac{S-M}{M} \times 100\%$ |
| 0             | 0.00                           | 209.40                                    | 209.40     | 0.00                         | 209.40         | 0.00                         |
| 1             | 1.83                           | 208.01                                    | 208.22     | 0.10                         | 208.02         | 0.00                         |
| 3             | 5.48                           | 198.33                                    | 198.79     | 0.23                         | 197.00         | -0.68                        |
| 5             | 9.13                           | 180.22                                    | 179.91     | -0.17                        | 174.95         | -3.01                        |
| 7             | 12.78                          | 152.27                                    | 151.61     | -0.44                        | 141.88         | -7.32                        |
| 9             | 16.43                          | 124.12                                    | 113.87     | -9.00                        | 97.79          | -26.92                       |
| 11            | 20.08                          | 86.86                                     | 66.69      | -                            | -              | -                            |
| 13            | 23.74                          | 59.91                                     | -          | -                            | -              | -                            |
| 15            | 27.39                          | 59.77                                     | -          | -                            | -              | -                            |
| 17            | 31.04                          | 68.98                                     | -          | -                            | -              | -                            |

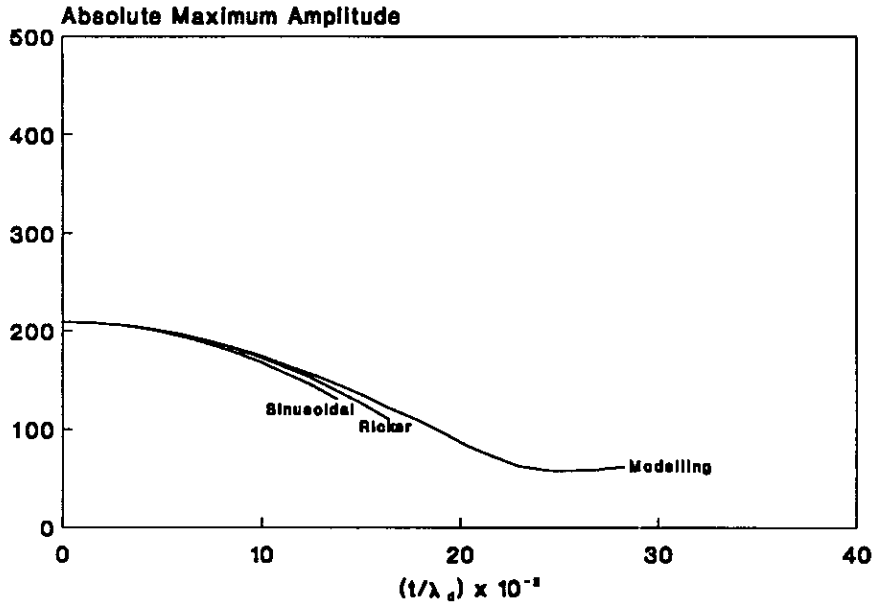


FIG. 6a The amplitude response for model 1D with a Ricker 18 Hz input wavelet whose maximum amplitude is 1000.

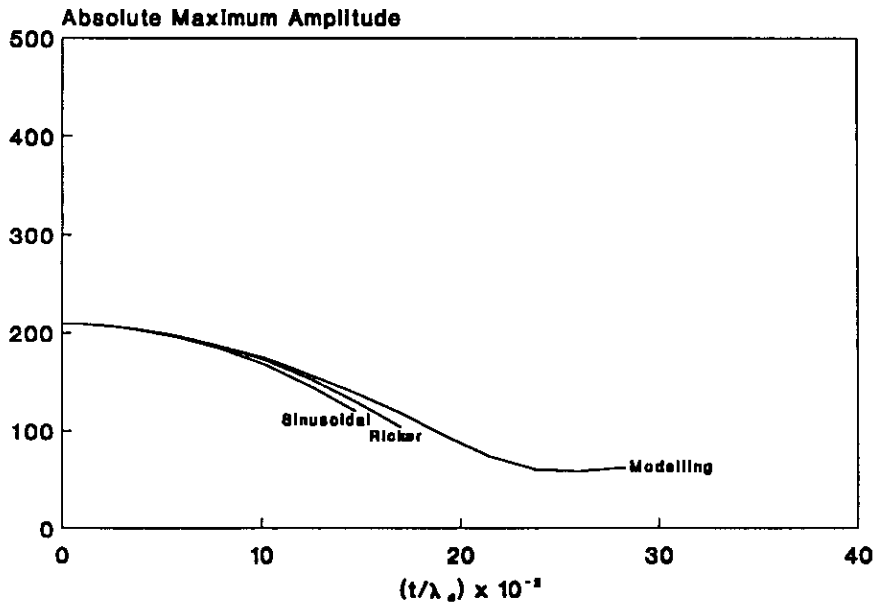


FIG. 6b The amplitude response for model 1D with a Ricker 31 Hz input wavelet whose maximum amplitude is 1000.

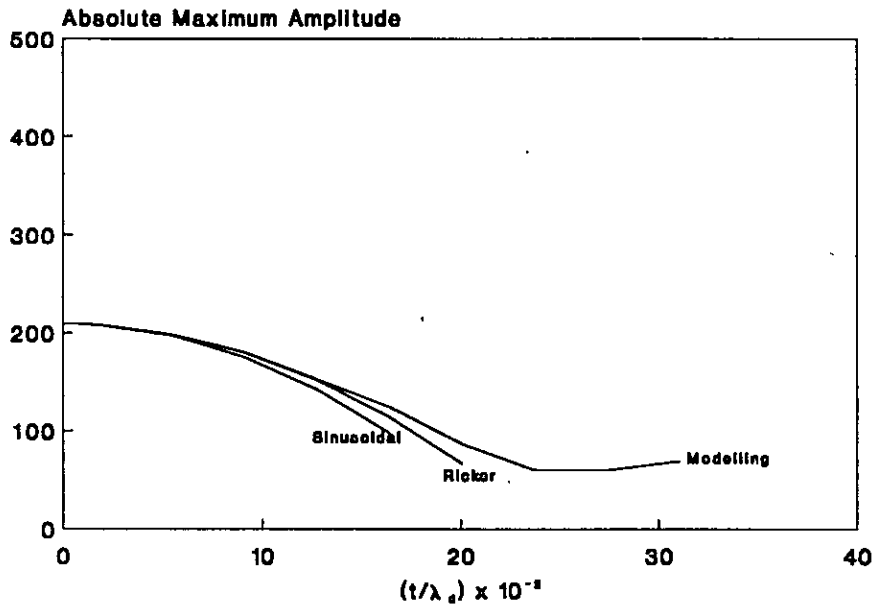
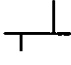


FIG. 6c The amplitude response for model 1D with a Ricker 50 Hz input wavelet whose maximum amplitude is 1000.

In Tables 4a, 4b and 4c, the modelling results are listed together with the results from the two approximations. They are also plotted in Figures 6a, 6b and 6c. Note that both the sinusoidal and Ricker approximations agree very well with the modelling results, as indicated by both the error calculations in Table 4 and Figure 6, for all three input wavelets. This implies that the two expressions for  $A_0$  and  $A_1$  are independent of frequencies. Note that the modelling results agree better with the Ricker approximation than with the sinusoidal approximation. This is to be expected since the input wavelets for the models are all zero-phase Ricker wavelets. However, the differences are very small. At  $(1/8)\lambda_d$  thickness, both approximations deviate much less than 10% from the modelling results. In fact, the Ricker approximation does not exceed 10% error until the thickness is roughly  $(0.16)\lambda_d$ . At about  $(1/4)\lambda_d$  thickness, tuning is also observed. In this case, it is a minimum, and the wavelet basically exhibits a flat spot at this thickness (trace 20, Figure 4d). Note that as the thickness increases further, the wavelet splits into two wavelets. Beyond this point if we measure the amplitude along the same time line along which the maximum is measured before the flat spot occurs, there is actually no tuning, i.e. a trough starts to occur along that time line. The amplitude increase for thicknesses larger than  $(1/4)\lambda_d$  is actually measured in one of two splitted wavelets.

One can conclude that for situations represented by model 1D, both the Ricker approximation and the sinusoidal approximations are good approximations for the amplitude response of a thin bed as a function of its thickness. If the input wavelet is indeed a Ricker wavelet, the Ricker approximation gives better results. In reality, one seldom knows the exact input wavelet, and the sinusoidal approximation may be used to obtain some reasonable results.

### Opposite Polarity and Unequal Magnitude

This case can be subdivided into two cases and are referred to as models 1B and 1C. They both represent the situation of a thin bed overlain and underlain by higher-velocity half-spaces whose velocities are different. They are similar to model 1A except that their two reflection coefficients have different magnitudes. For model 1B,  $r_1 = -0.1371$  and  $r_2 = 0.2272$ ; for model 1C,  $r_1 = -0.2072$  and  $r_2 = 0.1371$ . While model 1A is the most studied thin-layered situation, models 1B and 1C probably represent more common geological situations. However, in terms of amplitude and frequency analyses, models 1B and 1C are equivalent models. Mathematically, one can interchange  $r_1$  and  $r_2$  in equations (14) and (15) without affecting the results. Since  $|r_1|$  and  $|r_2|$  of model 1B are equal to  $|r_2|$  and  $|r_1|$  of model 1C respectively, they are identical in the applications of equations (14) and (15). In actual modelling, they are also equivalent for amplitude and frequency studies. The reason is as follows: Model 1B can be represented symbolically as . As shown earlier, it can be decomposed as the sum of an opposite-polarity and equal-magnitude term and an equal-polarity and equal-magnitude term:

$$-r_1 \begin{array}{|c|} \hline | \\ \hline \end{array} \begin{array}{|c|} \hline r_2 \\ \hline \end{array} = -r_3 \begin{array}{|c|} \hline | \\ \hline \end{array} \begin{array}{|c|} \hline r_3 \\ \hline \end{array} + r_4 \begin{array}{|c|} \hline | \\ \hline \end{array} \begin{array}{|c|} \hline r_4 \\ \hline \end{array}$$

$$\text{where } r_3 = \frac{r_2 + r_1}{2} \text{ and } r_4 = \frac{r_2 - r_1}{2}$$

Similarly, model 1C can be decomposed as:

$$-r_2 \begin{array}{|c|} \hline | \\ \hline \end{array} \begin{array}{|c|} \hline r_1 \\ \hline \end{array} = -r_5 \begin{array}{|c|} \hline | \\ \hline \end{array} \begin{array}{|c|} \hline r_5 \\ \hline \end{array} + -r_6 \begin{array}{|c|} \hline | \\ \hline \end{array} \begin{array}{|c|} \hline -r_6 \\ \hline \end{array}$$

$$\text{where } r_5 = \frac{r_1 + r_2}{2} \text{ and } r_6 = \frac{r_2 - r_1}{2}$$

Hence,  $r_3 = r_5$  and  $r_4 = r_6$ . The only difference is that the equal polarity terms for the two models are of opposite polarities. The convolution of a zero-phase wavelet with the opposite polarity terms in both models give a  $90^\circ$ -phase wavelet which is anti-symmetric about  $t = 0$ , taking  $t = 0$  to be at the centre between the two reflection spikes. For model 1B, the equal polarity term gives a normal polarity zero-phase wavelet to be added onto the anti-symmetry  $90^\circ$ -phase wavelet; for model 1C, a reverse polarity zero-phase wavelet is added. The result is that, if one performs a polarity reversal of the reflected composite wavelet of model 1B, it becomes the mirror image of model 1C about  $t = 0$ . In fact, if we perform a polarity reversal directly on the reflection spikes of model 1B, they become mirror image of the reflection spikes of model 1C. Note that the argument also holds for an input  $90^\circ$ -phase wavelet. Since we are here only interested in the absolute maximum amplitude, the two models will give identical results. For this reason, it is sufficient to run only one of the models for the amplitude study. Model 1B is arbitrarily chosen.

Table 5 Comparison of Modelling Data with Ricker and Sinusoidal Approximation for Model 1B at 31 Hz Peak Frequency ( $\lambda_d = 75.63$  m)

| Thickness (m) | $(t/\lambda_d) \times 10^{-2}$ | Absolute Maximum Amplitude (Input = 1000) |               |                            |                         |               |                            |
|---------------|--------------------------------|---|---------------|----------------------------|-------------------------|---------------|----------------------------|
|               |                                | Zero-Phase Input Wavelet                  |               |                            | 90°-Phase Input Wavelet |               |                            |
|               |                                | Ricker (R)                                | Modelling (M) | $\frac{R-M}{M} \times 100$ | Sinusoidal (S)          | Modelling (M) | $\frac{S-M}{M} \times 100$ |
| 0             | 0.00                           | 70.10                                     | 70.10         | 0.00                       | 70.10                   | 70.10         | 0.00                       |
| 1             | 1.32                           | 73.10                                     | 75.45         | -3.21                      | 75.49                   | 76.16         | -0.89                      |
| 3             | 3.97                           | 93.74                                     | 102.63        | -9.48                      | 109.44                  | 111.82        | -2.17                      |
| 5             | 6.61                           | 125.28                                    | 135.62        | -8.25                      | 156.71                  | 158.30        | -1.01                      |
| 7             | 9.26                           | 161.56                                    | 166.45        | -3.03                      | 208.53                  | 201.06        | 3.58                       |
| 9             | 11.90                          | 200.14                                    | 198.39        | -0.87                      | 262.34                  | 246.39        | 6.08                       |
| 11            | 14.54                          | 240.07                                    | 223.31        | -6.98                      | 317.28                  | 281.95        | 11.11                      |
| 13            | 17.19                          | -   | 242.93        | -                          | -                       | 310.00        | -                          |
| 15            | 19.83                          | -   | 257.75        | -                          | -                       | 330.99        | -                          |
| 17            | 22.48                          | -   | 265.67        | -                          | -                       | 341.68        | -                          |
| 19            | 25.12                          | -   | 268.36        | -                          | -                       | 344.07        | -                          |
| 21            | 27.77                          | -   | 266.76        | -                          | -                       | 339.38        | -                          |
| 23            | 30.41                          | -   | 260.98        | -                          | -                       | 326.37        | -                          |

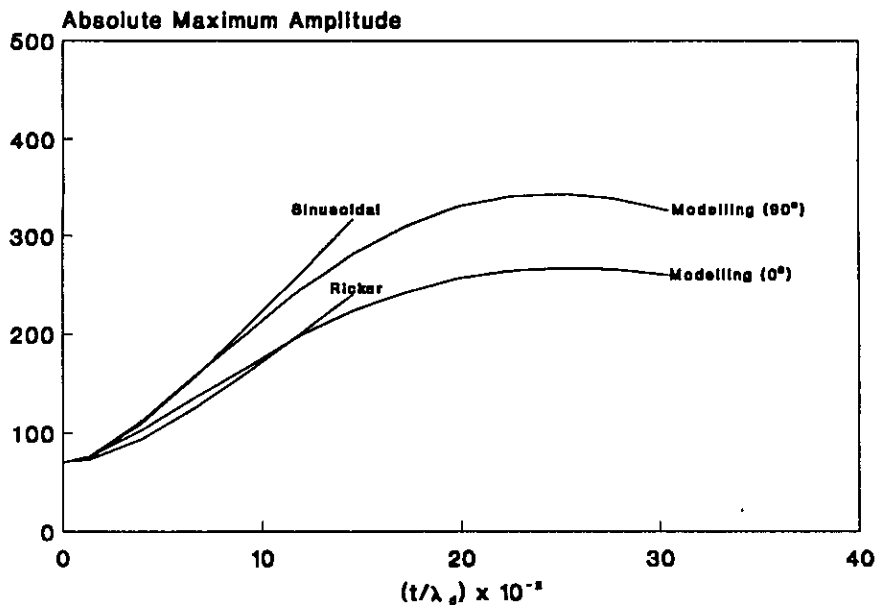


FIG. 7 The amplitude response for model 1B with Ricker 31 Hz input wavelets whose maximum amplitudes is 1000.

Table 5 lists the results of equations (14) and (15) alongside the modelling results. It shows that the percentage error between the Ricker approximation and the zero-phase modelling results are consistently larger than the percentage error between the sinusoidal approximation and the 90°-phase modelling results for thicknesses below the  $(1/16)\lambda_d$  value. As in model 1A, this is probably due to ignoring  $O(\Delta t^2)$  term in the derivation of the opposite polarity term in equation (14), when, in fact, the modelling involves the input wavelet trough area which requires terms of  $O(\Delta t^2)$  to describe its effects. However, for both approximations, the percentage errors do not exceed 10% until the thickness exceeds roughly the  $(1/8)\lambda_d$  value. The results are also plotted in Figure 7. Tuning occurs at  $(1/4)\lambda_d$  thickness. This is to be expected since model 1B can be expressed as a linear supposition of model 1A and model 1D. It is interesting to note that, although the Ricker approximation deviates from the modelling results more than the sinusoidal approximation does for small thicknesses, it agrees with the modelling results for larger thicknesses than that of the sinusoidal approximation. This implies that the thin-bed assumption is a more stringent assumption for the sinusoidal approximation than it is for the Ricker approximation.

### Equal Polarity and Unequal Magnitude

This case can also be subdivided into two cases and are referred to as model 1E and 1F. They both represent the situation of a thin bed overlain by a lower-velocity half-space and underlain by a higher-velocity half-space. They are similar to model 1D except that their two reflection coefficients have different magnitudes. For model 1E,  $r_1 = 0.0596$  and  $r_2 = 0.1494$ , and can be symbolically be represented as  $\underline{\uparrow}\uparrow$ . For model 1F,  $r_1 = 0.1371$  and  $r_2 = 0.0722$ , and can be symbolically be represented as  $\underline{\downarrow}\downarrow$ . As for models 1B and 1C, they can also be decomposed into an opposite-polarity and equal-magnitude term and an equal-polarity and equal-magnitude term. For example, both models 1E and 1F can be decomposed as follows:

$$r_1 \underline{\uparrow}\uparrow r_2 = -r_3 \underline{\uparrow}\uparrow r_3 + r_4 \underline{\downarrow}\downarrow r_4$$

$$\text{where } r_3 = \frac{r_2 - r_1}{2} \text{ and } r_4 = \frac{r_2 + r_1}{2}$$

Unlike models 1B and 1C,  $r_1$  and  $r_2$  of model 1E are not equal to  $r_2$  and  $r_1$  of model 1F respectively. However, the possible decompositions of both of them into two similar terms imply that the investigation of the amplitude properties of one of them is sufficiently representative of any two reflection spikes of equal polarity and different magnitudes. Model 1E is arbitrarily chosen for the study.

Table 6 and Figure 7 show the modelling results for model 1E alongside the results for the two approximations. The two approximations give practically identical results, which agree very well with the modelling results for thicknesses up to and slightly beyond the  $(1/8)\lambda_d$  value. Note that at a thickness of  $(1.3/10)\lambda_d$ , the percentage errors between

the approximations and the modelling results are only roughly 5%. Note also that the results of models 1D and 1E, and hence any two reflection spikes of equal polarity, can be better approximated with the two approximations than the opposite-polarity cases. The reason is because, for equal-polarity cases, the contribution from the opposite-polarity term in equations (14) and (15) are very small, and hence the problem of neglecting  $O(\Delta t^2)$  as mentioned several times earlier is minimal. Tuning occurs also at  $(1/4)\lambda_d$  thickness, which is a direct consequence of the fact that, as shown by model 1D, the equal-polarity term tunes at  $(1/4)\lambda_d$ , and the contribution from the opposite-polarity term is minimal, though it also tunes as a maximum at  $(1/4)\lambda_d$  thickness.

Table 6 Comparison of Modelling Data with Ricker and Sinusoidal Approximations for Model 1E at 31 Hz Peak Frequency ( $\lambda_d = 83.20$  m)

| Thickness<br>(m) | $(t/\lambda_d) \times 10^{-2}$ | Absolute Maximum Amplitude (Input = 1000) |               |                              |                   |                              |
|------------------|--------------------------------|---|---------------|------------------------------|-------------------|------------------------------|
|                  |                                | Modelling<br>(M)                          | Ricker<br>(R) | $\frac{R-M}{M} \times 100\%$ | Sinusoidal<br>(S) | $\frac{S-M}{M} \times 100\%$ |
| 0                | 0.00                           | 209.00                                    | 209.00        | 0.00                         | 209.00            | 0.00                         |
| 1                | 1.20                           | 208.59                                    | 208.53        | -0.03                        | 208.51            | -0.04                        |
| 3                | 3.61                           | 205.14                                    | 204.81        | -0.16                        | 204.65            | -0.24                        |
| 5                | 6.01                           | 198.42                                    | 197.42        | -0.51                        | 197.04            | -0.70                        |
| 7                | 8.41                           | 188.82                                    | 186.51        | -1.24                        | 185.96            | -1.54                        |
| 9                | 10.82                          | 177.99                                    | 172.35        | -3.27                        | 171.92            | -3.53                        |
| 11               | 13.22                          | 163.67                                    | 155.42        | -5.31                        | 155.89            | -4.99                        |
| 13               | 15.63                          | 151.33                                    | -             | -                            | -                 | -                            |
| 15               | 18.03                          | 139.15                                    | -             | -                            | -                 | -                            |
| 17               | 20.43                          | 129.29                                    | -             | -                            | -                 | -                            |
| 19               | 22.84                          | 124.51                                    | -             | -                            | -                 | -                            |
| 21               | 25.24                          | 122.79                                    | -             | -                            | -                 | -                            |
| 23               | 27.64                          | 123.80                                    | -             | -                            | -                 | -                            |
| 25               | 30.04                          | 126.48                                    | -             | -                            | -                 | -                            |



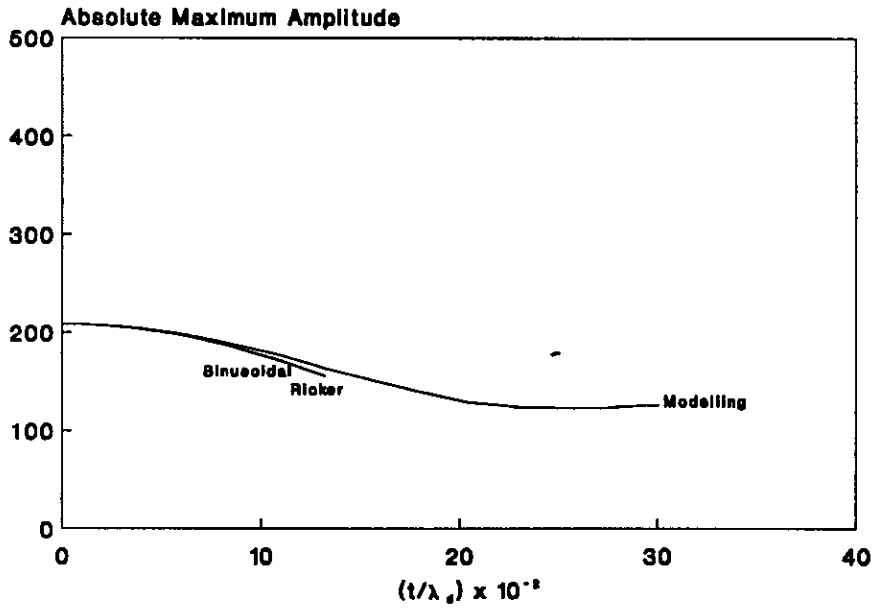


FIG. 8 The amplitude response for model 1E with a Ricker 31 Hz input wavelet whose maximum amplitude is 1000.

## DISCUSSION

From our analysis, several conclusions can be drawn. The first conclusion is that the opposite-polarity and equal-magnitude case is a singular case in that it is the only case where the amplitude response as a function of thickness is a linear function under the thin-bed assumption. All other cases are complex second-ordered polynomials. The second conclusion is that the sinusoidal approximation is a reasonable approximation for the Ricker zero-phase wavelet, and an excellent approximation for the Ricker 90°-phase wavelet. This is a significant point, since in real data, we do not know the exact wavelet. But if the sinusoidal approximation is a good approximation for the Ricker wavelets, it is likely a good approximation for any zero-phase and/or 90°-phase looking wavelet. The third conclusion is that for amplitude study, a 90°-phase wavelet input may be preferable to a zero-phase wavelet input due to the problem of incongruous wavelet mixing as explained in fig. 2. Consequently, the amplitude response as a function of the bed thickness has a higher gradient for a 90°-phase input wavelet than that for a zero-phase input wavelet. Hence, amplitude changes as a function of the bed thickness would be more observable on data with a 90°-phase wavelet input than that with a zero-phase wavelet input for the same range of thickness.

Equations (14) and (15) can be used in forward modelling to deduce the lithology of a thin layer. For example, the velocity of the thin layer can be varied in these equations until the corresponding curves agree with the observed results on the real data. They can also be used to calibrate real data in development situations where the zero limit of the reservoir rock is needed to be mapped from seismic data. At present, using the same approach, we are studying the properties of two thin layers. It will be interesting to see how the results differ from that of a single layer.

## REFERENCES

- Berkout, A.T., 1984, Seismic resolution: Geophysical Press Ltd., 16-33
- de Voogd, N. and den Rooijen, H., 1983, Thin-layer response and spectral bandwidth: *Geophysics* 48, 12-18.
- Gardner, G.H.F., Gardner, L.W. and Gregory, A.R., 1974, Formation velocity and density - the diagnostic basics for stratigraphic traps: *Geophysics* 39, 770-780.
- Koefoed, O. and de Voogd, N., 1980, The linear properties of thin layers, with an application to synthetic seismograms over coal seams: *Geophysics* 45, 1254-1268.
- Widess, M.B., 1973, How thin is a thin bed?: *Geophysics* 38, 1176-1180.